

Mode-locked fiber laser in the C-band region for dual-wavelength ultrashort pulses emission using a carbon nanotube saturable absorber

Kuen Yao Lau (刘坤耀)¹, Pin Jern Ker (郭炳仁)¹, Ahmad Fauzi Abas²,
Mohammed Thamer Alresheedi², and Mohd Adzir Mahdi^{3,*}

¹Electronics Research Group, Institute of Power Engineering, Universiti Tenaga Nasional, 43000 Kajang, Selangor, Malaysia

²Department of Electrical Engineering, College of Engineering, King Saud University, Riyadh 11421, Kingdom of Saudi Arabia

³Wireless and Photonics Networks Research Centre, Faculty of Engineering, Universiti Putra Malaysia, 43400 UPM Serdang, Selangor, Malaysia

*Corresponding author: mam@upm.edu.my

Received December 1, 2018; accepted January 30, 2019; posted online May 8, 2019

A saturable absorber is commonly employed to generate an ultrashort laser with a mode-locking scheme. In an erbium-doped fiber laser system, the laser regimes of either 1530 or 1550 nm wavelength are procured based on the absorption profile of the erbium-doped fiber. The absorption of the erbium-doped fiber is designed to emit at both wavelengths by controlling the net gain of the laser cavity. Subsequently, simultaneous erbium-doped fiber laser emission is attained at 1533.5 and 1555.1 nm with the pulse duration of 910 and 850 fs, respectively. Therefore, this work maximizes the output portfolios of a mode-locking fiber laser for dual-wavelength ultrashort pulses emission.

OCIS codes: 140.3538, 190.7110, 320.7090.
doi: 10.3788/COL201917.051401.

The fast growing adaption of the fiber laser in industry has appeared to be the alternative technology to prior art, solid-state lasers. There are two categories of fiber lasers: continuous wave and pulsed fiber lasers. This work focuses on the latter category on generating ultrashort pulses, termed as mode-locked fiber laser (MLFL). A technique to generate MLFL is the integration of a saturable absorber (SA) inside the fiber laser cavity. In a laser cavity, the SA transmits light at high excitation intensities with reduced optical loss when the initial states of the absorbing transition are empty, and the final states are fully occupied. This phenomenon is dubbed as saturable absorption, which occurs in a medium with strong absorbing dopant ions.

Numerous technologies have been proposed with saturable absorption properties, such as a semiconductor SA mirror (SESAM) and integrating materials with fiber end facets or microfibers. However, SESAM requires stringent and complicated fabrication facilities that spur researchers to investigate fiber-based SAs. The integrated materials in a fiber-based SA include a carbon nanotube (CNT), graphene, transition metal dichalcogenides, topological insulator, phosphorene, gold nanorods, and lately graphene-oxide carboxylic acid^[1-6]. Despite being an extensively studied material since 2004 for the first SA demonstration by Set *et al.*^[7], the progress of a CNT-SA for a dual-fiber laser at a near 1.55 μm wavelength emission with femtosecond pulses is limited. Most CNT-SAs deploy the sandwiched structure in a dual-wavelength

mode-locked laser, which shows the limitation of low thermal damage threshold. Therefore, a tapered fiber CNT-SA was demonstrated for the generation of a dual-wavelength MLFL with better thermal management^[8]. However, the pulse duration of a 1533 nm mode-locked laser was attained at 1.06 ps in Ref. [8]. In order to generate dual-wavelength MLFL, net gain cross section variation is demonstrated by changing cavity losses^[8,9] or monitoring the pump power^[10]. In addition, two chirped fiber Bragg gratings with a 1 and 6 nm bandwidth, respectively are used to divide the mode-locked laser into two regions at around 1550 nm^[11].

In this work, we propose a solution of generating two mode-locked laser outputs with closely spaced operating wavelengths using a tapered fiber CNT-SA. The tapered fiber CNT-SA possesses insertion losses of 2.46 dB at 1550 nm and a modulation depth of 2.5%, in conjunction with our previous works in Refs. [12,13]. The laser cavity is designed with the implementation of a red/blue wavelength division multiplexer (R/B-WDM), which splits the laser propagation into two separate optical paths at wavelengths near 1530 and 1550 nm. This work presents the dual-MLFL with the shortest pulse duration of 910 and 850 fs, pulse repetition rate of 10.47 and 10.89 MHz using CNT-SA with C-band emission wavelength at 1533.5 and 1555.1 nm, respectively. The dual-mode-locked lasers contribute to practical applications, such as asynchronous optical sampling, which operates with fixed pulse repetition rate difference as sources of

pump and probe pulses^[14], as well as the generation of dual-comb spectroscopy from two frequency combs with slightly different pulse repetition rates to achieve spectral resolution without frequency tuning^[15].

Figure 1 depicts the schematic diagram for dual-wavelength MLFL. A 980 nm laser diode (LD) is used to pump a section of 4.5 m erbium-doped fiber (EDF) with absorption of 3.5 dB/m and dispersion parameter of -18 ps/(nm·km) at 1550 nm via a wavelength division multiplexer (WDM). The SA is inserted before the R/B WDM-1. A similar tapered fiber CNT-SA is employed to our previous works^[12,13]. The R/B WDM-1 splits the optical signal into two paths; longer-wavelength MLFL (MLFL-L) path through polarization controller (PC-1) and shorter-wavelength MLFL (MLFL-S) path through PC-2. The PC is employed to adjust the cavity birefringence effect. The optical coupler (OC) acts as the coupling ratio splitting element into a portion of 70:30; 30% signal is extracted from the laser cavity for output (OP) measurement, and the remaining 70% signal reverts into the laser cavity. Both of the 70% signals from MLFL-L and MLFL-S are combined at R/B WDM-2. The propagating signal of the entire cavity is controlled by an isolator (ISO) in the forward pumping mechanism to achieve a complete laser oscillation system. The net group velocity dispersions for the MLFL-S and MLFL-L are deduced as -0.2338 and -0.2126 ps², which conclude the anomalous regime for both laser cavities.

Figures 2(a) and 2(b) show the optical spectrum of the proposed dual-wavelength MLFL. The measurement is obtained using a Yokogawa AQ6370B optical spectrum analyzer with 0.02 nm bandwidth resolution. The MLFL-S and MLFL-L are observed with the operating wavelength ranging from 1520 to 1540 nm and from 1545 to 1565 nm, respectively. Both MLFLs achieve the mode-locking pump power threshold at 15.4 mW. However, the mode-locked laser spectrum is slightly inconsistent in Fig. 2(a), when the measurement is taken at threshold power level due to the conversion from continuous wave laser to mode-locked laser with only sufficient pump power. At pump power more than 18.9 mW, a smooth optical spectrum is observed consecutively. On the other hand, a smooth optical spectrum is observed, even at 15.4 mW threshold pump power in Fig. 2(b). This is attributed to the higher gain in the longer wavelength

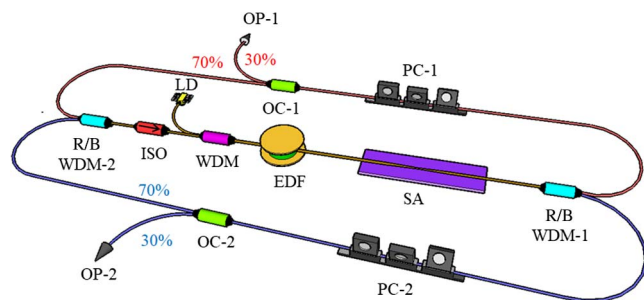


Fig. 1. Experimental setup for dual-wavelength MLFL.

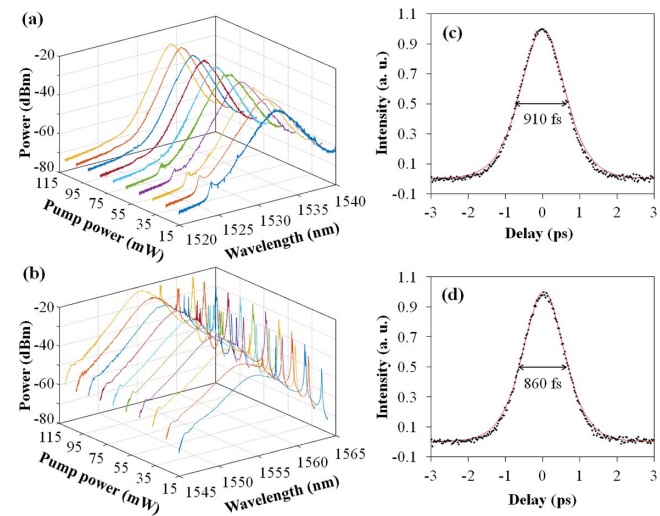


Fig. 2. Optical spectra for (a) MLFL-S and (b) MLFL-L and autocorrelation traces for (c) MLFL-S and (d) MLFL-L.

region near 1550 nm, in conjunction with a low average population inversion operating regime^[16]. However, the mode-locked laser spectrum is slightly inconsistent for MLFL-L at higher pump power, which could be due to the generation of multiple pulsing^[17,18]. In this work, dual-wavelength emission near 1530 and 1550 nm is observed due to the separation of C-band emission through R/B WDM-1. The mode-locking operation is investigated until the maximum pump power of 110.3 mW. At this pump power, the central wavelength (λ_c) and spectral bandwidth ($\Delta\lambda$) for MLFL-S are 1533.5 and 2.7 nm. Contrarily, λ_c and $\Delta\lambda$ for MLFL-L are measured at 1555.1 and 3.9 nm. The peak power increases from -36.1 to -26.6 dBm at the central wavelength of 1533.5 nm and from -38.3 to -20.8 dBm at the central wavelength of 1555.1 nm when the pump power is raised from 15.35 to 110.3 mW. The observation of Kelly sidebands validates the MLFL operation in the soliton regime. A soliton is invulnerable to a variety of distortions^[19]. Therefore, a stable pulse with soliton operation can be readily formed despite discrete amounts of dispersion and nonlinearity in the entire laser cavity^[20].

The ultrashort pulse measurement of MLFLs is conducted with an autocorrelator based on second harmonic generation, as depicted in Figs. 2(c) and 2(d). The measurement is taken at the maximum pump power of 110.3 mW. Based on Figs. 2(c) and 2(d), the pulse width is measured as 910 and 850 fs for MLFL-S and MLFL-L, respectively. The experimental measurement is curve fitted with a secant hyperbolic (sech^2) profile. The time bandwidth product of MLFL-S and MLFL-L is computed as 0.32 and 0.41, respectively, denoting that the pulse is slightly chirped. The chirping mechanism can be compensated by optimizing the dispersion of the MLFL-L.

The pulse train of the MLFL is investigated with a 1.25 GHz bandwidth oscilloscope and a 1.5 GHz photo-detector. The measurement is conducted at 110.3 mW

maximum pump power, as portrayed in Figs. 3(a) and 3(b). The pump power at 110.3 mW is sufficient to generate multiple soliton pulses^[13]. The generation of multiple soliton pulses is also supported by high nonlinearity of the CNT-SA, as well as the strong light–matter interaction between the tapered fiber and the CNT nanomaterial. However, only a single pulse is perceptible in both MLFL-S and MLFL-L instead of multiple pulses, whereby the latter pulse regime could feasibly occur. This might be limited by the resolution of the oscilloscope, which could not resolve the closely spaced multiple pulses. The multiple pulses phenomena were thoroughly presented in Refs. [17,18]. Fundamental pulses are attained for both MLFL-S and MLFL-L with the repetition rate of 10.47 and 10.89 MHz, respectively. This repetition rate corresponds to the cavity length of 19.63 m for MLFL-S and 18.87 m for MLFL-L. The absence of chaotic multiple pulses moving in random configuration from the oscilloscope trace validates the high stability of MLFLs. The radio frequency (RF) spectrum of the mode-locked pulses is illustrated in Figs. 3(c) and 3(d). The peak-to-background ratio (PBR) of the MLFL-S and MLFL-L is obtained as 45.7 and 44.0 dB, respectively. These values are comparable to the reported PBR in Ref. [21].

The power development curve of the MLFL is presented in Fig. 4(a). Based on these findings, the laser pump power

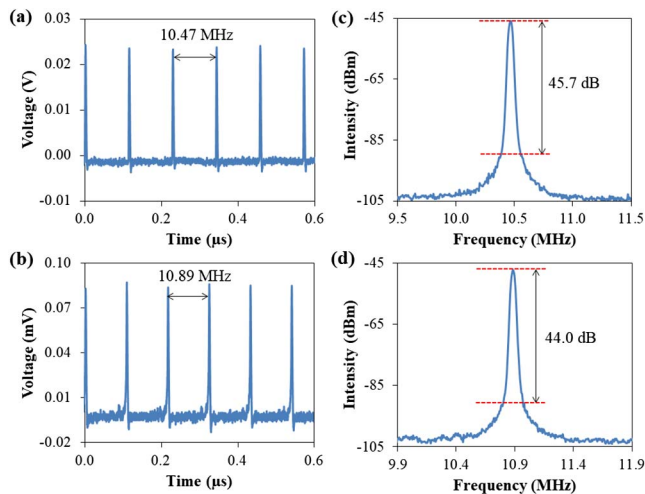


Fig. 3. Pulse trains for (a) MLFL-S and (b) MLFL-L and RF spectra for (c) MLFL-S and (d) MLFL-L.

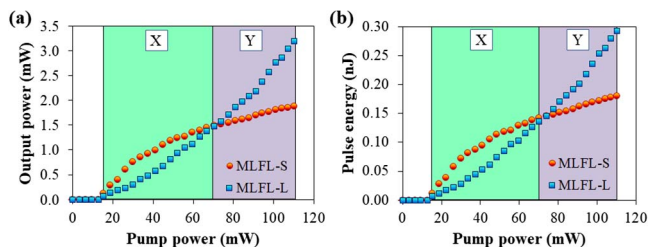


Fig. 4. Power development curves for (a) MLFL-S and (b) MLFL-L.

threshold is observed at 15.3 mW for both lasers. The relationship between output power and pump power is not exactly linear. In Region X, MLFL-S presents higher output power than MLFL-L. This is attributed to the gain properties of erbium ions, whereby the gain coefficient for MLFL-S is higher than that of MLFL-L. Contrarily, MLFL-L shows higher output power than MLFL-S in Region Y. This is owing to the saturation factor, in which the MLFL-S reaches its saturation faster than the MLFL-L. However, the total output power by summing both MLFL-S and MLFL-L shows a linear relationship as a function of pump power, which is in agreement with the laser theory. At maximum pump power, the average output power is achieved at 1.88 and 3.19 mW for MLFL-S and MLFL-L, respectively. The computed laser slope efficiencies of MLFL-S are 2.69% in Region X and 0.99% in Region Y. On the other hand, MLFL-L recorded slope efficiencies of 2.58% and 4.41% in Region X and Region Y, respectively. This measurement is in agreement with the spectral evolution in Figs. 2(a) and 2(b), in which the peak power of MLFL-L is more pronounced at higher pump power. The pulse energy is deduced by dividing the average output power to pulse repetition rate, as depicted in Fig. 4(b). The maximum pulse energy is recorded at 0.18 and 0.29 nJ for MLFL-S and MLFL-L, respectively. Subsequently, the slope efficiencies for pulse energy of MLFL-S and MLFL-L are 0.18% and 0.31%, respectively. Overall, MLFL-L possesses higher output power than MLFL-S due to the aforementioned factors in optical spectrum analysis.

The stability evaluation of the output pulses from MLFL-S and MLFL-L over 60 min observation duration is depicted in Fig. 5. The measurement is recorded at the maximum pump power of 110.3 mW. Based on the findings, the mode-locking operation of both laser cavities is maintained throughout the observation time without any significant distortions on the spectrum.

The summary of dual-MLFL emission employing CNT-SA is tabulated in Table 1. Improvement is awarded by the laser cavity design in this work that generates two laser outputs in contrast to Refs. [8–11]. Apart from that, dual-MLFL emission is obtained with both femtosecond pulse duration in comparison to Ref. [8] and shorter than Ref. [11].

In conclusion, we have demonstrated a simple solution of generating a dual-wavelength MLFL implementing a tapered fiber CNT-SA. The dual-wavelength mode-locking laser is emitted at two different C-band wavelengths using

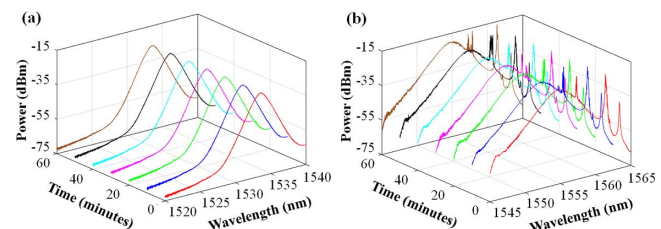


Fig. 5. Stability evaluation for (a) MLFL-S and (b) MLFL-L.

Table 1. Summary of Dual-MLFL Emission Using CNT-SA

Ref.	Laser Output	Wavelength (nm)	Pulse Duration (fs)
[8]	One	1533.0 1560.0	1060 734
[9]	One	1531.0 1557.0	1310 1360
[10]	One	1548.6 1551.2	6000 5700
[11]	One	1532.2 1557.3	990 950
This work	Two	1533.5 1555.1	910 850

an R/B WDM. The MLFL at a shorter wavelength centered at 1533.5 nm generates a spectral bandwidth of 2.7 nm, pulse duration of 910 fs, repetition rate of 10.47 MHz, and PBR of 45.7 dB. The second mode-locked laser is attained at a center wavelength of 1555.1 nm, spectral bandwidth of 3.9 nm, pulse duration of 850 fs, repetition rate of 10.89 MHz, and PBR of 44.0 dB. This work contributes to doubling the femtosecond laser outputs to conventional technology for diverse applications in energy, materials or photonics, and optics.

We would like to express our sincere appreciation to Dr. Khanh Kieu, University of Arizona, for fabricating the CNT-SA sample in this work. The authors extend their appreciation to the International Scientific Partnership Program ISPP at King Saud University for funding this research work through ISPP#0106.

References

1. M. Akhtar, G. Anderson, R. Zhao, A. Alruqi, J. E. Mroczkowska, G. Sumanasekera, and J. B. Jasinski, *NPJ 2D Mater. Appl.* **1**, 5 (2017).
2. M. Liu, A. Luo, W. Xu, and Z. Luo, *Chin. Opt. Lett.* **16**, 020008 (2018).
3. F. Zhao, Y. Wang, Y. Wang, H. Wang, and Y. Cai, *Chin. Opt. Lett.* **15**, 101402 (2017).
4. X. Wang, N. Zhao, H. Liu, R. Tang, Y. Zhu, J. Xue, Z. Luo, and W. Xu, *Chin. Opt. Lett.* **13**, 081401 (2015).
5. Y. Chen, G. Jiang, S. Chen, Z. Guo, X. Yu, C. Zhao, H. Zhang, Q. Bao, S. Wen, D. Tang, and D. Fan, *Opt. Express* **23**, 12823 (2015).
6. C. Zhao, H. Zhang, X. Qi, Y. Chen, Z. Wang, S. Wen, and D. Tang, *Appl. Phys. Lett.* **101**, 211106 (2012).
7. S. Y. Set, H. Yaguchi, Y. Tanaka, and M. Jablonski, *J. Light. Technol.* **22**, 51 (2004).
8. A. A. Latif, H. Mohamad, M. H. Abu Bakar, F. D. Muhammad, and M. A. Mahdi, *Laser Phys.* **26**, 025106 (2016).
9. X. Zhao, Z. Zheng, L. Liu, Y. Liu, Y. Jiang, X. Yang, and J. Zhu, *Opt. Express* **19**, 1168 (2011).
10. D. Han and C. Zeng, *Opt. Commun.* **319**, 25 (2014).
11. Y. C. Kong, H. R. Yang, W. Li, and G. W. Chen, *Laser Phys.* **25**, 015101 (2014).
12. K. Y. Lau, E. K. Ng, M. H. Abu Bakar, A. F. Abas, M. T. Alresheedi, Z. Yusoff, and M. A. Mahdi, *Opt. Commun.* **413**, 249 (2018).
13. K. Y. Lau, E. K. Ng, M. H. Abu Bakar, A. F. Abas, M. T. Alresheedi, Z. Yusoff, and M. A. Mahdi, *Opt. Laser Technol.* **102**, 240 (2018).
14. A. Bartels, R. Cerna, C. Kistner, A. Thoma, and F. Hudert, *Rev. Sci. Instrum.* **78**, 035107 (2007).
15. S. Schiller, *Opt. Lett.* **27**, 766 (2002).
16. N. A. M. A. Hambali, M. A. Mahdi, M. H. Al-Mansoori, M. I. Saripan, and A. F. Abas, *Appl. Opt.* **48**, 5055 (2009).
17. M. Liu, Z.-R. Cai, S. Hu, A.-P. Luo, C.-J. Zhao, H. Zhang, W.-C. Xu, and Z.-C. Luo, *Opt. Lett.* **40**, 4767 (2013).
18. A.-P. Luo, M. Liu, X.-D. Wang, Q.-Y. Ning, W.-C. Xu, and Z.-C. Luo, *Photon. Res.* **3**, A69 (2015).
19. Y.-H. Lin, C.-Y. Yang, S.-F. Lin, and G.-R. Lin, *Opt. Mater. Express* **5**, 236 (2015).
20. A. Luo, P. Zhu, H. Liu, X. Zheng, N. Zhao, M. Liu, Z. Luo, and W. Xu, *Opt. Express* **22**, 175 (2014).
21. A. Martinez, K. Fuse, B. Xu, and S. Yamashita, *Opt. Express* **18**, 23054 (2010).